ARTICLE

Gel breakdown in a formulated product via accumulated strain – Supplementary Information

Andrew Clarke,

Experimental

Rheometry

The step stress experiment reported in the main text (Fig. 10) was acquired at the limit of capability of the rheometer. The twin-drive version of the MCR702 separates the applied strain (lower drive) from the measured torque (upper drive) hence the response is faster than a single drive stress-controlled instrument. Nevertheless, the instrument is seen to reach within 5% of target shear-rate (5.11s^{-1}) at a strain of about 5%, Figure S 1.

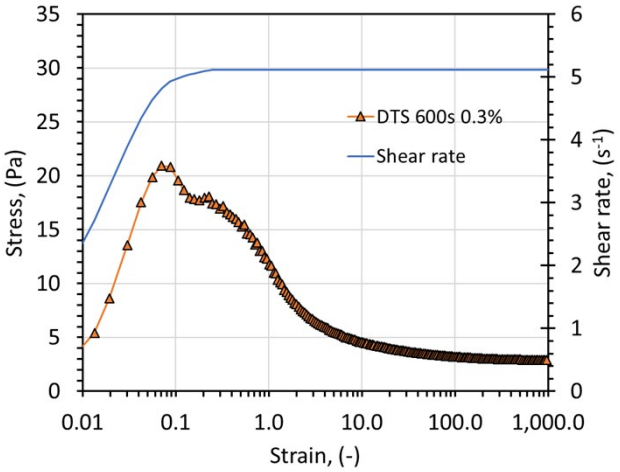

Figure S 1 Simultaneously recorded shear rate and stress as a function of strain during one step shear rate experiment.

To further investigate the presence of the observed peak at about 8% strain we plot the step shear-rate experiment performed at a sequence of increasing shear-rates, Figure S 2. Although the peak is less prominent at lower rates than at 5.11s^{-1}, there is a clear shoulder that persists. In Figure S 2b we plot the recorded shear rate as a function of strain, here normalised to the target shear rate. At 1s^{-1} the instrument is within 5% of the target shear-rate already at 2% strain.

Figure S 3a shows how the step shear-rate stress overshoot peak varies for various amplitude oscillation measurement during the waiting time. Again the sample was reset using 1000s^{-1} shear-rate for 5min followed by a SAOS / MAOS measurement at the specified strain amplitude for 600s followed by a step shear-rate experiment at 1s^{-1}. At small amplitudes a shoulder at approx. 10% strain is present. In Figure S 3b we illustrate the dependence of stress overshoot on sample age. In each case the sample was subject to a SAOS measurement at 0.3% amplitude 10 rad s^{-1} during the waiting period.

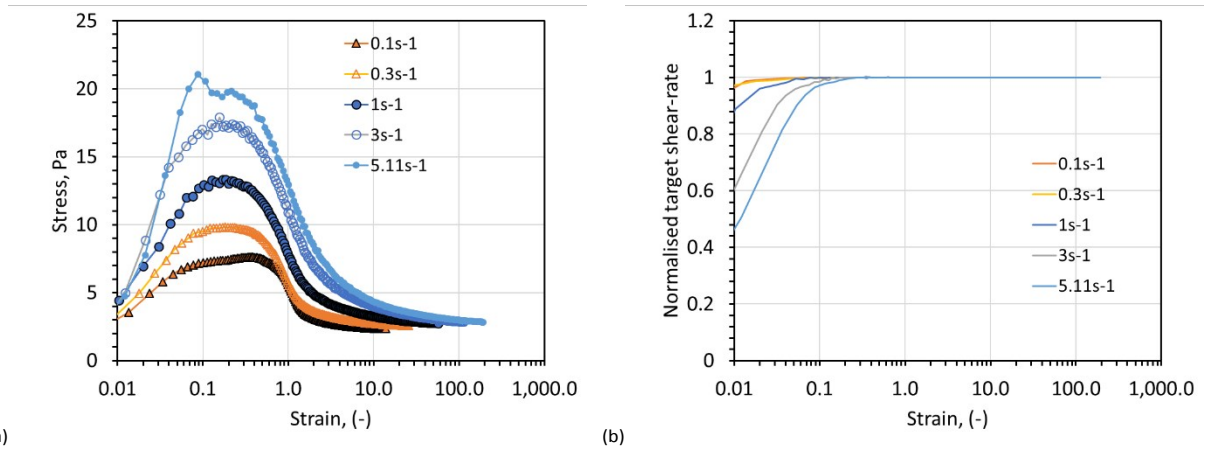

(a) (b)

Figure S 2 (a) Step shear-rate experiments at a variety of shear rates. In each case the sample was reset with a preshear of 1000s^{-1} for 5mins and a wait period of 300s during which the sample moduli were measured with an oscillation strain amplitude of 0.3% and frequency of 10 rad s^{-1}. (b) Simultaneously recorded approaches to target shear rate normalised by the target rate.

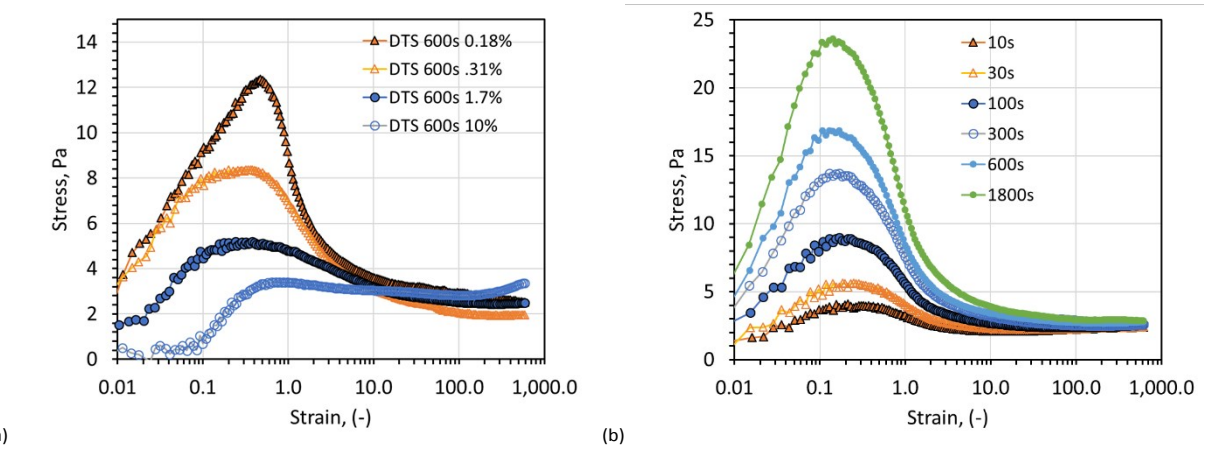

(a) (b)

Figure S 3 (a) Step shear-rate experiments at 1s^{-1} for a sample aged 600s during which varying amplitude oscillation experiments are performed (10rad s^{-1}). (b) Step shear-rate experiments at 1s^{-1} illustrating the dependence of stress overshoot dependence on sample age.

An alternative protocol to evolve gel structure has been reported by Moghimi et al[1] whereby the gel is pre-sheared at different strain amplitudes and then on cessation of flow probe how the elasticity and its magnitude measured in the linear regime evolves with time. This experiment for higher amplitude preshear is shown in Figure S 4. In this case the modulus was probed with an oscillation of 0.25% strain amplitude and a frequency of 10 rad s^{-1} and the LAOS preshear step was applied for 200s, after 5min at 1000s^{-1} steady shear reset.

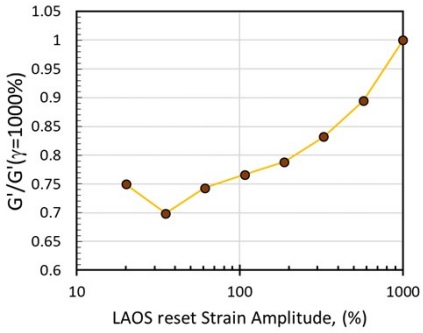

Figure S 4 Effect of large amplitude oscillatory shear to reset gel structure. The modulus at a sample age of 300s is plotted normalised by the value obtained with 1000% LAOS preshear,

The strain stiffening ratio, *S*, and shear thickening ratio, *T*, are defined by Ewoldt et al[2] as,

$$S \equiv \frac{G'_L - G'_M}{G'_L} = \frac{4e_3 - 4e_5}{e_1 + e_3 + e_5} \quad \text{* MERGEFORMAT (1)}$$

$$T \equiv \frac{\eta'_L - \eta'_M}{\eta'_L} = \frac{4\upsilon_3 - 4\upsilon_5}{\upsilon_1 + \upsilon_3 + \upsilon_5} \quad \text{* MERGEFORMAT (2)}$$

with moduli, e_n and v_n defined in terms of the response harmonic structure as,

$$e_n = G'_n \cdot i^{(n-1)} \quad \text{* MERGEFORMAT (3)}$$

$$v_n = G''_n / \omega \quad \text{* MERGEFORMAT (4)}$$

The data of Figure S 5 in the main text are reproduced in Figure S 5a below. In Figure S 5b are shown the corresponding strain-stiffening ratio plots and in Figure S 5c the corresponding shear-thickening ratio plots. S and T were calculated from data to 5th harmonic.

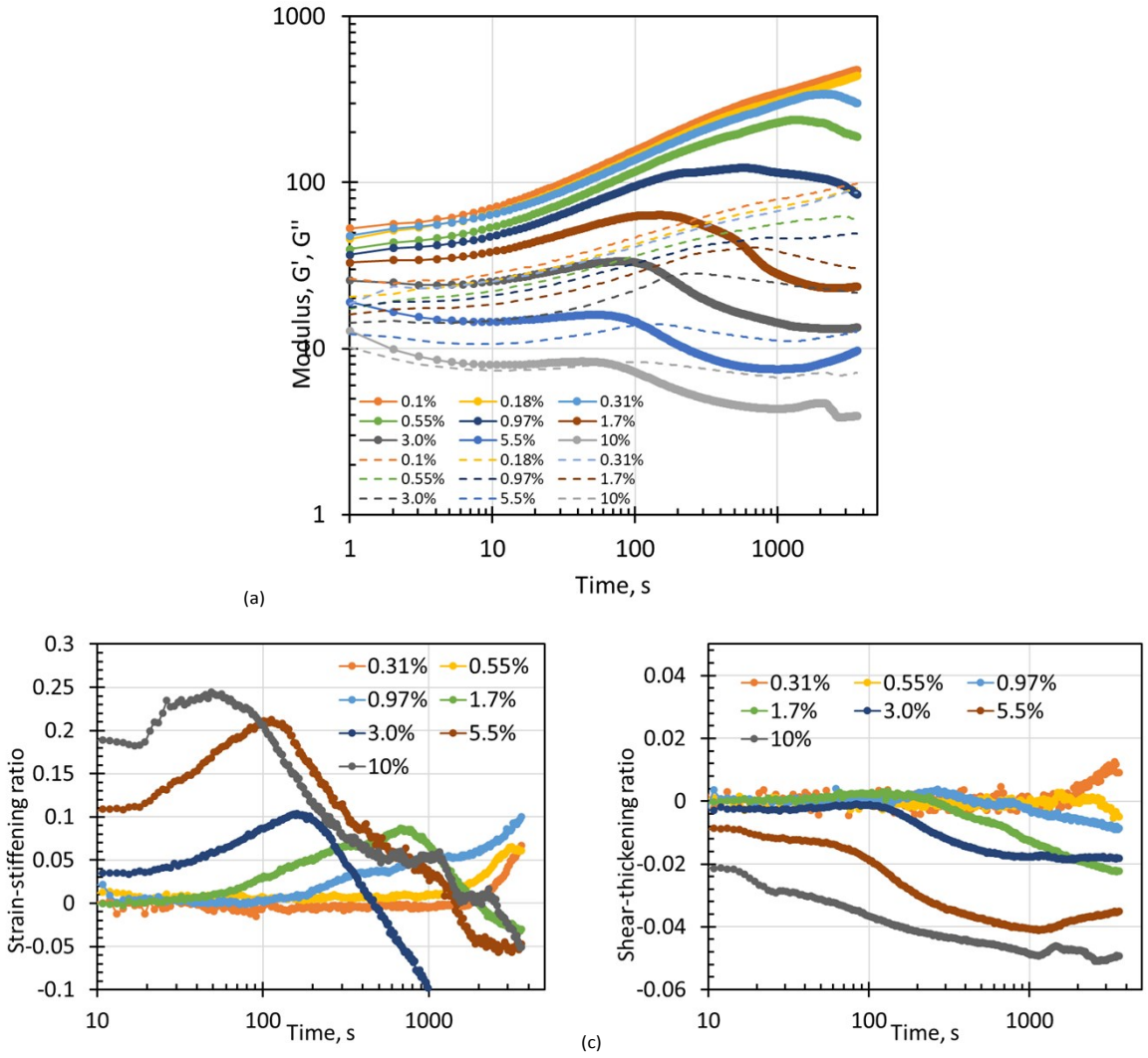

Figure S 5 (a) Small and medium amplitude oscillation dynamic time sweeps. Solid symbols G', open symbols G''. Figure 5 in main text. (b) Strain-stiffening ratio, S. (c) Shear-thickening ratio, T.

In the main text, Fig. 8b shows the evolving Cole-Cole plot[3] of the intra-cycle transient $G'_t(t)$ and $G_t''(t)$ for a 1.7% perturbation. Figure S 6 shows the corresponding plot for an oscillation strain amplitude of 10%. The deltoid even at 10s exhibits crossing of the $G'_t(t) = G_t''(t)$ line and thus is associated with intracycle fluidisation. This corresponds to the finite values seen in the strain-stiffening and shear thickening ratios in Figure S 5.

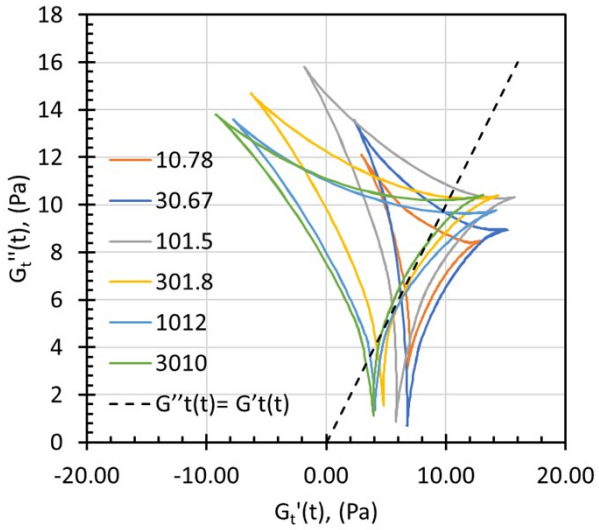

Figure S 6 SPP analysis cole-cole plot for at the elapsed times, in seconds, shown in the legend along the evolution at a strain amplitude of 10%.

Gel Collapse

The gel column height was measured in transmission using a Turbiscan™ instrument. Here we see a delay-time until a free oil (continuous phase) is seen. This measurement was made with a sample temperature of 65°C as with rheological measurements. The sample was pre-sheared, in this case using a high-shear mixer (Silverson LR4T), and then loaded into a sample vial suitable for the instrument. The height of the interface between the gel and the free oil layer is plotted as a function of time in Figure S 7. Initially there is no free oil layer, then after about 2 days the gel begins to collapse and a free oil layer is observed.

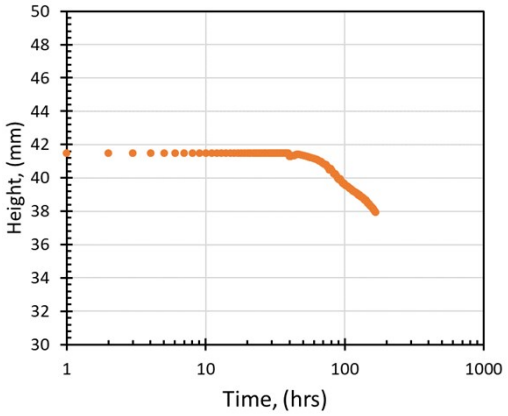

Figure S 7 Observed gel column height as a function of time. The gel is seen to start collapsing after approximately 2 days.

Molecular Modelling

There have been a host of studies of evolution of attractive gels in the literature[4-7]. These papers make use of an open source general purpose molecular modelling package (LAMMPS[8] – Large-scale Atomic/Molecular Massively Parallel Simulator; https://lammps.sandia.gov). We have set up a simulation of a large number of particles interacting via a Morse potential in a 3D geometry and have evolved the system in time subject to certain physical conditions. Whereas the chosen model is simplistic compared to a drilling fluid, we expect to gain insight into structures formed in the fluid under varying conditions.

The LAMMPS Model

We use Langevin dynamics which models interactions through a background implicit solvent. Note that the solvent provides a viscous damping on the particle motion only; there are no background hydrodynamics modelled. The model is a Brownian dynamics simulation and the force on each particle has the form,

$$F = F_c + F_f + F_r \qquad \text{* MERGEFORMAT (5)}$$

with F_c the conservative force between particles calculated with a chosen particle interaction potential, F_f is a frictional drag (i.e. viscous damping) proportional to the particle's velocity, and F_r is a random force due to solvent molecules, at temperature T, randomly bumping into the particle.
We model F_c with a Morse potential so that,

$$F_c = \frac{\partial U}{\partial r}; \quad U = U_0\left[e^{-2k(r-2a)} - 2e^{-k(r-2a)}\right] \quad r < r_c \qquad \text{* MERGEFORMAT (6)}$$

The model is run with dimensionless units. A unit cell with periodic boundaries in x, y and z is set up with a regular array of 50x50x49 = 122500 particles. T is initially set to 0.5 and the system equilibrated to randomise the motion of the particles. Then the temperature is reduced to $T = 0.2$ so that U_0 is $5k_BT$ as used in Padmanabhan et al.[7] Temperature is monitored and the system allowed to randomise at the elevated temperature for time $50t_0$. The temperature is then reduced, and the system allowed to relax for a further $200t_0$ Figure S 8 and Figure S 9.

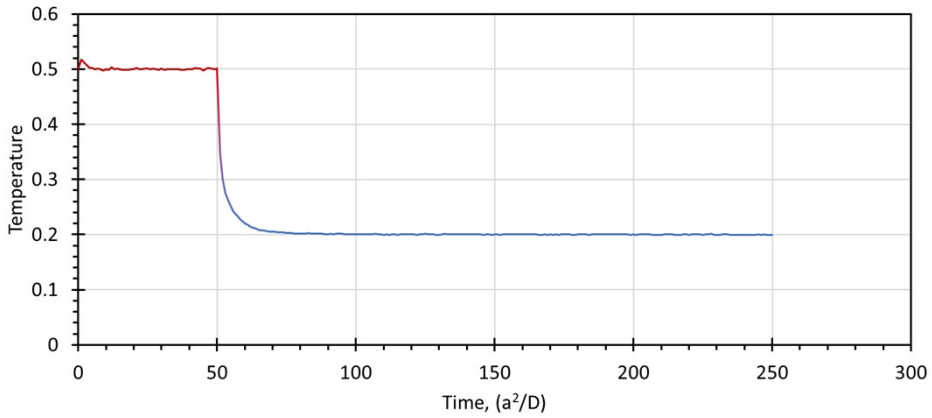

Figure S 8 Non-dimensionalised system temperature as a function of time.

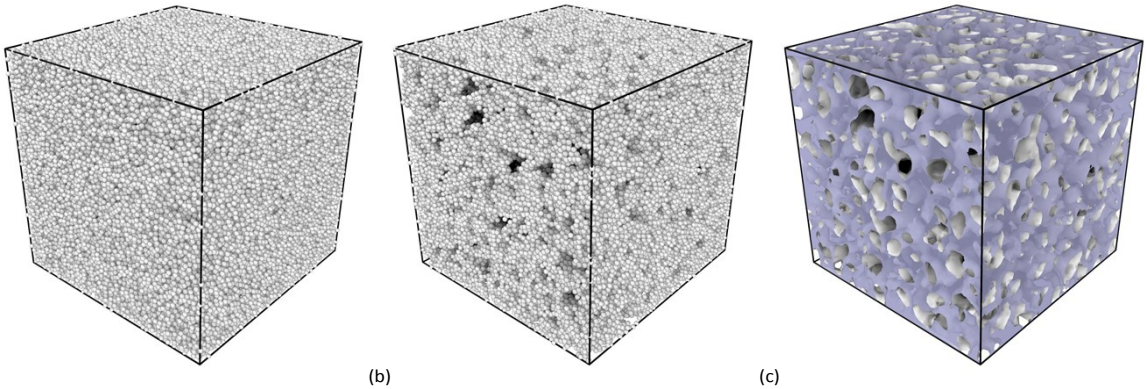

(a) (b) (c)

Figure S 9 (a) Thermalized initial state $50t_0$, (b) cooled and equilibrated state, $250t_0$, (c) particle distribution from (b) rendered with a constructed surface mesh from which surface area and enclosed volume can be calculated.

Structure evolution

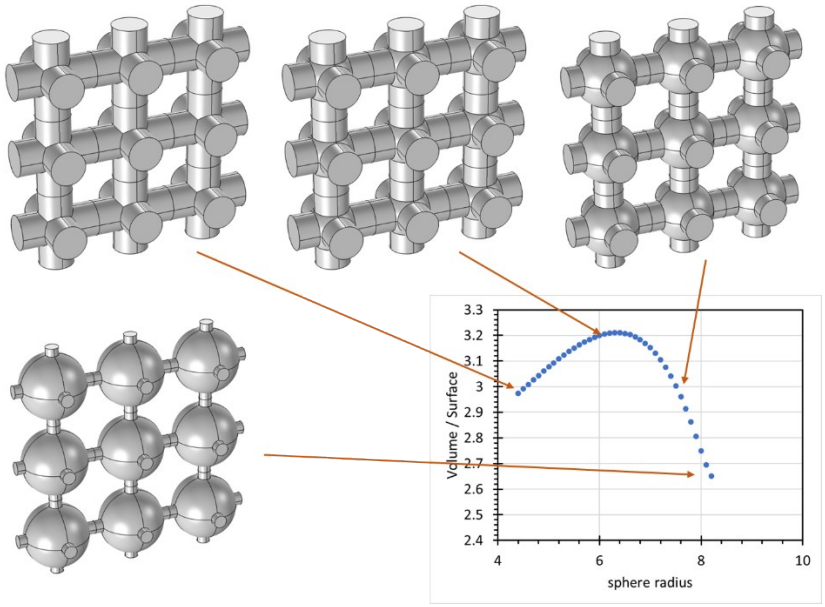

Figure S 10 Simple conceptualisation of monotonic evolution of structure leading to peak in volume to surface ratio. Shapes calculated for constant enclosed volume.

We choose to characterise the aggregated structure using a simple volume to surface area ratio of the network formed. We use the open visualisation tool Ovito[9] to construct the surface mesh from which network volume and surface area are calculated[10]. A simple ratio of volume enclosed to surface area provides a lengthscale characterising the structure. We envisage that the structure initially evolves as described by Padmanabhan[7], with particles diffusing from "strands" to "nodes", Figure S 10. With a constant enclosed volume, this evolution leads to an initially increasing volume to surface ratio followed by a decreasing ratio as the structure evolves from rods to spheres. Eventually though, we might expect that both the unit cell grows and the strands break so that the "nodes" become isolated spheres. Over extended times the LAMMPS model evolves in the same qualitative manner and the volume to surface ratio steadily increases with the structure overall exhibiting bigger holes and fewer strands. Note that we have not run the *quiescent* simulation for sufficient time to observe a subsequent drop in the volume to surface ratio.

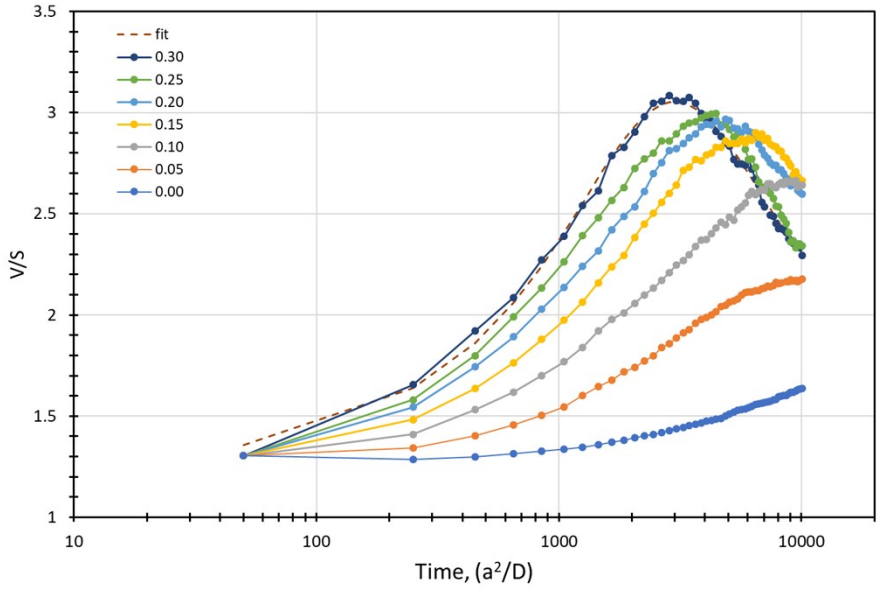

Figure S 11 Volume to surface ratio for varying amplitude strain as a function of time. The curves are fitted with an arbitrary function (logarithmically scaled Lorentzian) to systematically extract the peak position. The peak positions are plotted in the main text figure 13.

In Figure S 11 we show the evolution of V/S for a sequence of oscillating strain amplitudes. In each case the data were fitted with an arbitrarily chosen function (logarithmically scaled Lorentzian) and the peak position extracted. The peak positions are plotted in figure 13 of the main text.

Shear induced evolution

Having prepared the system, a sinusoidal perturbation of amplitude γ_0 is applied to mimic the SAOS experimental protocol. The amplitude, γ_0, and frequency, ω, can be adjusted. In the LAMMPS code we use the "fix deform wiggle" command to deform the unit cell with period $100t_0$ with no volume change. The shear strain is determined by the command whilst the shear-stress is calculated using the zero temperature virial definition[4],

$$\sigma_{xy} = \frac{1}{V}\sum_{i=1}^{N}\frac{\partial U}{\partial r_i^x}r_i^y \qquad \text{* MERGEFORMAT (7)}$$

The stress-strain relationship defines the modulus of the system. Thus, provided the strain amplitude is sufficiently small that linear deformations only are considered, the complex modulus ($G^*=G'+iG''$) is determined by fitting with,

$$\sigma_{xy}(t) = \gamma_0\left(G'(\omega,\gamma_0)\sin(\omega t) + G''(\omega,\gamma_0)\cos(\omega t)\right) \qquad \text{* MERGEFORMAT (8)}$$

In applying this fit it is important to understand that it is only expected to be valid for linear stress-strain regions. The evolution of the Lissajous-Bowditch curves as a function of the applied strain amplitude is shown in Figure S 12. The maximal linear strain amplitude was determined to be 1.15%.

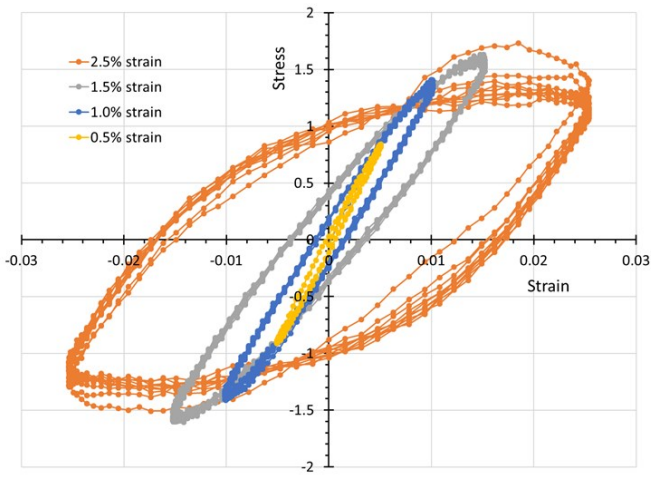

Figure S 12 Evolution of the Lissajous-Bowditch curves as a function of strain amplitude for the LAMMPS calculation.

Notes and references

1. E. Moghimi, A. R. Jacob, N. Koumakis and G. Petekidis, *Soft Matter*, 2017, **13**, 2371-2383.
2. R. H. Ewoldt, A. E. Hosoi and G. H. McKinley, *Journal of Rheology*, 2008, **52**, 1427-1458.
3. S. A. Rogers, *Rheologica Acta*, 2017, **56**, 501-525.
4. C. Ferreiro-Cordova, E. Del Gado, G. Foffi and M. Bouzid, *Soft Matter*, 2020, **16**, 4414-4421.
5. L. C. Johnson, B. J. Landrum and R. Zia, *Soft Matter*, 2018, DOI: 10.1039/c8sm00109j.
6. L. C. Johnson, R. N. Zia, E. Moghimi and G. Petekidis, *Journal of Rheology*, 2019, **63**, 583-608.
7. P. Padmanabhan and R. Zia, *Soft Matter*, 2018, **14**, 3265-3287.
8. S. Plimpton, *J. Comp. Phys*, 1995, **117**, 1-19.
9. Ovito can be found at https://www.ovito.org/
10. A. Stukowski, *Jom*, 2013, **66**, 399-407.